# Co-Optimization of Long Secondary Double-Sided Linear Flux Switching Permanent Magnet Motors

Cheng Wen[1,*], Jian Cui[1], Mingye Li[2], Zhiping Wan[1], and Yujian Chang[1]

[1]*Hebei Provincial Collaborative Innovation Center of Transportation Power Grid Intelligent Integration Technology and Equipment, School of Electrical and Electronic Engineering, Shijiazhuang Tiedao University, Hebei 050043, China*
[2]*The School of Network and Communication, Hebei Polytechnic Institute, Shijiazhuang, Hebei 050091, China*

**ABSTRACT:** This study aims to achieve the co-optimization of thrust force and thrust fluctuation using a long secondary double-sided linear flux switching permanent magnet motor (LSDLFSPM). Firstly, the motor model is constructed and derived using a theoretical approach. Subsequently, the motor parameters are subjected to sensitivity analysis using the Taguchi method to identify the significant influencing factors. Based on the screening results, the Response Surface Method (RSM) is employed to construct the test space and derive regression equations for thrust force and thrust fluctuation. The Multi-Objective Grasshopper Optimization Algorithm (MOGOA) is then utilized to iteratively optimize the regression equation for optimal parameter sizes. Finally, the optimized results are validated through finite element analysis (FEA) and compared with the original motor performance to demonstrate the effectiveness of the optimization approach proposed in this paper.

## 1. INTRODUCTION

With the development of industrial technology, the application of linear motors is becoming increasingly widespread. LSDLFSPM, a high-efficiency drive device, exhibits excellent performance and has a wide range of application scenarios. However, the fluctuation of thrust generated during motor operation affects the stability and accuracy of the motor's performance [1]. The thrust force, which serves as the driving force of motor operation, also influences the operating efficiency of the motor. As the motor thrust force increases, there is a corresponding increase in thrust fluctuations, which further impact the stable operation of the motor. Therefore, it is crucial to conduct co-optimization of motor thrust force and thrust fluctuations.

The optimal design of electric motors often starts with optimizing structural parameters to enhance the motor's overall performance, but this is a complex process with multiple parameters and unknown influences on performance. Intelligent optimization algorithms in motor optimization overcome traditional shortcomings and improve design efficiency. In [2], Taguchi method screens significant factors for a permanent magnet linear synchronous motor (PMLSM) and combines the Kriging model with a multi-objective particle swarm optimization (MOPSO) algorithm to enhance the comprehensive motor performance. In [3], in order to address the problems of parameter sensitivity and high thrust fluctuation of double-side linear vernier permanent magnet motors (DS-LVPM), RSM with an improved differential evolutionary algorithm is used to form a multi-objective optimization framework to optimize the parameters of the motors. In [4], sensitivity analysis and multi-objective genetic algorithm achieve the global optimization of

a complementary and modular linear flux-switching permanent magnet motor (CMLFSPM), reducing detent force. In [5], Kriging models and improved genetic algorithm (GA) optimize parameters for a doubly-fed linear motor (DFLM) subsection, and FEA verifies the improved method. In [6], machine learning and multi-objective optimization reduce optimization effort for homopolar linear synchronous motors (HLSMs) and improve accuracy. In [7], significant parameters of the motor are optimized using multi-objective GA considering the multiplicity of effects on the single-sided linear induction motors (SLIMs), which substantially reduces the normal force of the motor. In [8], introducing Bayesian Optimization (BO) and Hyper Band (HB) into the random forest regression algorithm (RF) to improve the prediction accuracy of the model as well as combining it with the second-generation non-dominated sorting genetic algorithm (NSGA-II) for multi-objective optimization improves the output performance of flux-switching linear motors.

In this study, Taguchi's method is used to screen significant factors and reduce the complexity of structural parameter optimization. RSM is employed to establish the test space and regression model, which is then combined with MOGOA for synergistic optimization of thrust force and thrust fluctuation through a comprehensive optimization method.

The paper is organized as follows. Section 2 develops the simulation model of LSDLFSPM and derives the theoretical model of thrust force and thrust fluctuation. Section 3 utilizes Taguchi method to screen significant structural parameters. Section 4 uses RSM to build the experimental design space for significant parameters and the regression model. Section 5 combines the regression model with MOGOA for iterative optimization, solving for optimal structural parameter sizes. Fi-
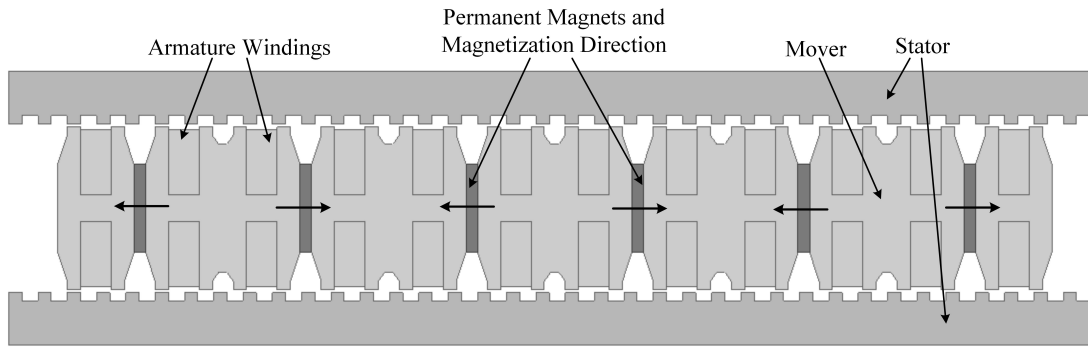
---

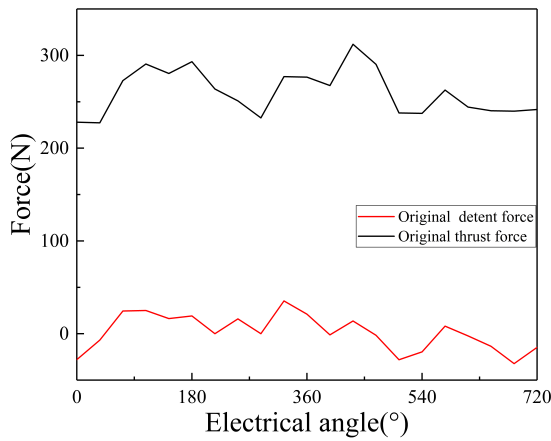**FIGURE 1**. LSDLFSPM topologies.



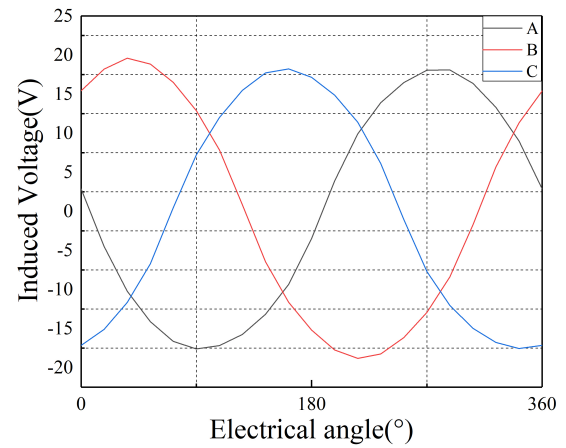**FIGURE 2**. Initial thrust force and detent force.



**FIGURE 3**. Initial no-load induced voltage.

nally, motor performances before and after optimization are compared using FEA to illustrate the effectiveness of structural parameter optimization in this study.

## 2. MODEL CONSTRUCTION

### 2.1. Initial Model

The LSDLFSPM has a spatially strict symmetrical structure, with the long stator consisting solely of an iron core, a short mover embedded with armature windings, and horizontally alternatingly magnetized permanent magnets. When operating, the motor is driven by the excitation of the short mover, which has advantages of simple structure and high thrust force, among others. The structure of the LSDLFSPM is shown in Fig. 1.

### 2.2. Initial Performance

Based on the initial structure of the LSDLFSPM topology, its initial performance is analyzed using FEA. In order to get more accurately analyzed results, the air gap width is divided into four layers.

The output thrust force and detent force of the LSDLFSPM under the initial structural parameters are shown in Fig. 2. The output average thrust force of the motor is 261.33 N; the thrust

fluctuation is 36.19%; and the detent force is 41.0034 N obtained from FEA.

The no-load induced voltage and harmonic analysis have a large impact on the operation and efficiency of the motor. The three phases A, B, C of the LSDLFSPM are 120° apart from each other with amplitudes of 18.11 V, 18.25 V, and 18.23 V, respectively, at the initial structural parameters. The positive and negative peaks of the waveforms in Fig. 3 show that the three-phase waveforms have a better symmetry. The no-load induced voltage of phase A in Fig. 3 is taken for harmonic analysis, and by calculation it is known that the harmonic distortion rate of phase A is 6.27%. The harmonic analysis is shown in Fig. 4.

The magnitude of the air gap flux density has a significant impact on the energy loss and operation of the motor. Compared to conventional permanent magnet linear motors, the LSDLFSPM's unique polymagnetization characteristics result in a higher air gap flux density. The peak air-gap magnetization of LSDLFSPM under four-layer air-gap grid dissection is 1.1 T. The variation of the air-gap magnetization over a distance of 350 mm of moving the motor is given in Fig. 5.

### 2.3. Theoretical Model

In this research, the thrust force and thrust fluctuation of LSDLFSPM are taken as optimization objectives. It is very im-
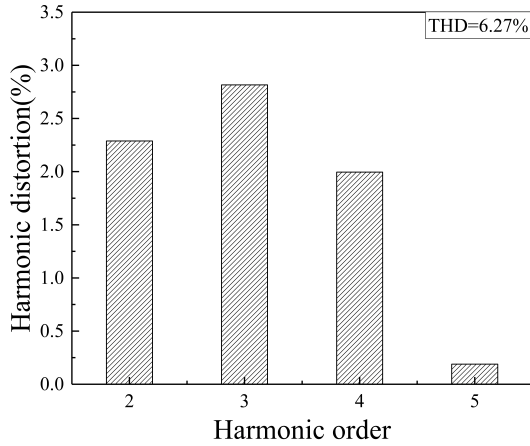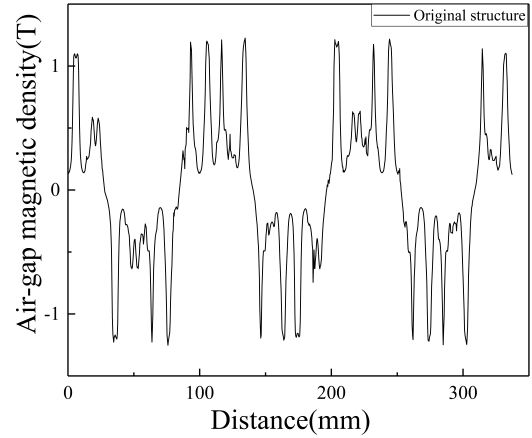
FIGURE 4. Initial A-phase harmonic analysis.



FIGURE 5. Initial air-gap magnetization density.

portant to determine factors affecting the thrust force and thrust fluctuation before carrying out the optimization. The thrust force of LSDLFSPM motor can be determined by combining the magnetic co-energy method, the work done by the thrust force, and the displacement of the motor motion [9, 10]:

$$F_e = \frac{dW_e}{dx_1}|_l = F_r + F_{pm} + F_{cog} \qquad (1)$$

where $x_1$ is the distance of motor movement; $W_e$ is the work done by the thrust force; $F_{pm}$, $F_r$, $F_{cog}$ are the permanent magnet thrust, reluctance component, and no-load detent force, which can also be expressed as:

$$F_{pm} = \frac{d}{dx_1}(\psi_{pm}^T I) = \frac{d\psi_{pma}}{dx_1}i_a + \frac{d\psi_{pmb}}{dx_1}i_b + \frac{d\psi_{pmc}}{dx_1}i_c$$
$$= \frac{3}{2}\frac{2\pi}{\tau_s}\psi_m I_m \cos\alpha = \frac{3\sqrt{2}}{2}\frac{\pi A_s l_m B_m l_a c_s k_d k_N \cos_\alpha}{m} \qquad (2)$$

$$F_r = \frac{1}{2}I^T \left(\frac{d}{dx_1}L\right)I \qquad (3)$$

$$F_{cog} = -\frac{d\psi}{dx_1}i = -R_g\phi\frac{d\phi}{dx_1} = -\frac{1}{2}\phi_m^2\frac{dR_g}{dx_1} \qquad (4)$$

This is obtained by collapsing the above equation:

$$F_e = \frac{1}{2}I^T \left(\frac{d}{dx_1}L\right)I + N_{pm}I\frac{d\phi_m}{dx_1} - \frac{1}{2}\phi_m^2\frac{dR_g}{dx_1} \qquad (5)$$

Through Eq. (5), it can be seen that the main factors affecting the thrust force of the LSDLFSPM are the armature current $I$, the structural parameters of the motor dimensions $l_m$, $l_a$, winding coefficients $k_d$, and leakage coefficients $k_N$. In the above equation, $B_m$ is the air-gap magnetic density; $\tau_s$ is the stator pole distance of the motor; $L$ is the inductance matrix; $I_m$ is the peak current; $i_a$, $i_b$, $i_c$ are the three-phase currents; $R_g$ is the air-gap magnetoresistance; $\phi_m$ is the air-gap magnetic flux; $\psi_{pm}$ is the permanent magnet flux matrix; $N_{pm}$ is the number

of turns per phase of winding. From this it is also possible to define the thrust fluctuation of the motor thought:

$$F_{rip} = \frac{F_{max} - F_{min}}{F_{avg}} \times 100\% \qquad (6)$$

Through the analysis of FEA and theoretical models, thrust force of the LSDLFSPM is related to the dimensions of the structural parameters and other factors, so it is feasible to carry out the optimization of structural parameters to improve the performance of the motor.

## 3. SIGNIFICANT INFLUENCE PARAMETERS SCREENING

LSDLFSPM motor has many structural design parameters, according to its flux switching principle and design principle, and the parameters can be categorized into fixed and adjustable ones.

The fixed parameters include stator pole pitch, mover pole pitch, winding phase spacing, mover tooth width, stator tooth width, etc., which are related to the basic attributes of the motor. In order to facilitate the optimization of the structural parameters, the air gap width is fixed at 1 mm in this paper. The widths of the teeth of the mover and stator are fixed at 4.455 mm, divided into fixed parameters. Adjustable parameters total 9, with specific labeling and initial dimensions, are shown in Figs. 6 and Table 1.

The number of LSDLFSPM adjustable structure parameters is large. How to effectively, with high efficiency, screen out the parameters that significantly affect the motor thrust force and thrust fluctuation is critical for carrying out the optimization design. Taguchi's method, a parameter sensitivity analysis technique, can be used to select different level combinations of parameters through fewer experimental designs, identifying parameters significantly influencing optimization objectives [11]. Nine adjustable parameters are set at three level values, establishing a 27-experiments space, as shown in Table 2.

The mean signal-to-noise (S/N) ratio is an important consideration for sensitivity analysis by Taguchi's method, whose
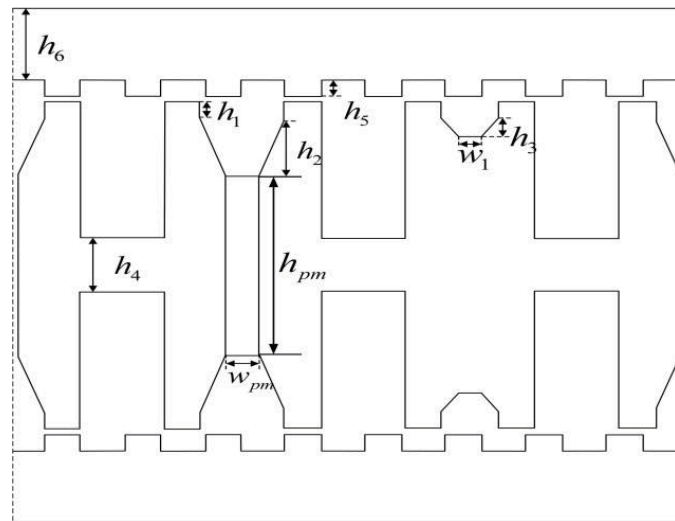
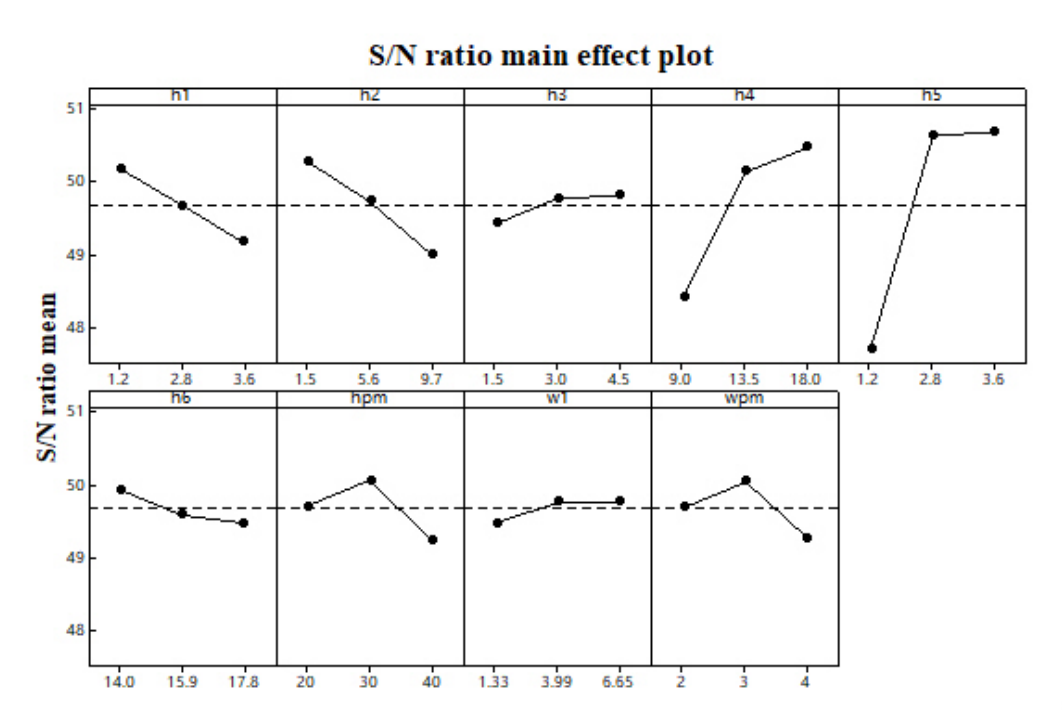**FIGURE 6**. Adjustable parameters marking.



**FIGURE 7**. S/N ratio mean.

magnitude is the key for screening and analyzing significant parameters. Based on the experimental data in Table 2, the mean value of S/N ratio is calculated for each parameter. In this paper, significant influence parameters are determined on the principle that the thrust force of the motor is expected to be large. Fig. 7 shows the effect diagram of S/N ratio.

From Fig. 7, it can be clearly seen that the nine adjustable parameters have average value of S/N ratio at the three set levels. The larger the value is, the more significant the effect of the parameter on the optimization objective is. The S/N ratios for the mover connection height $h_3$, mover connection width $w_1$, and stator yoke height $h_6$ have small mean values, reflect-

ing the small influence of these three parameters on the output thrust force of the motor, while the other six structural parameters have large mean values of the S/N ratios. According to this, the significant parameters are finally determined as follows $h_1$, $h_2$, $h_4$, $h_5$, $h_{pm}$, $w_{pm}$.

## 4. ESTABLISHMENT OF REGRESSION MODEL

Having determined the significant influence parameters of LS-DLFSPM, it is necessary to establish a test space for it to lay the foundation for the optimization design. In this research, RSM is used to establish the test space, and it can reduce the test space under consideration of the interaction of parameters.

**TABLE 1**. Adjustable parameter names and initial sizes.

| Names | Initial size (mm) |
|---|---|
| Mover tooth height $h_1$ | 2.8 |
| Mover bridge arms $h_2$ | 9.7 |
| Mover connection height $h_3$ | 3 |
| Mover yoke height $h_4$ | 9 |
| Stator tooth height $h_5$ | 2.8 |
| Stator yoke height $h_6$ | 17.8 |
| Mover connection width $w_1$ | 2.235 |
| Permanent magnet height $h_{pm}$ | 30 |
| Permanent magnet width $w_{pm}$ | 4 |

**TABLE 2**. Taguchi method experimental space.

| Tests | $h_1$ | $h_2$ | $h_3$ | $h_4$ | $h_5$ | $h_6$ | $w_1$ | $h_{pm}$ | $w_{pm}$ | $F_e$ | $F_{rip}$ |
|---|---|---|---|---|---|---|---|---|---|---|---|
| 1 | 1.2 | 40 | 9 | 4.5 | 3.99 | 5.6 | 2.8 | 17.8 | 3 | 305.35 | 0.4183 |
| 2 | 3.6 | 40 | 18 | 1.5 | 3.99 | 5.6 | 3.6 | 14 | 2 | 361.94 | 0.1806 |
| 3 | 3.6 | 20 | 9 | 3 | 6.65 | 5.6 | 3.6 | 14 | 3 | 303.55 | 0.4511 |
| ... | ... | ... | ... | ... | ... | ... | ... | ... | ... | ... | ... |
| 26 | 1.2 | 40 | 13.5 | 4.5 | 1.33 | 9.7 | 3.6 | 15.9 | 2 | 369.82 | 0.2507 |
| 27 | 2.8 | 30 | 18 | 1.5 | 3.99 | 1.5 | 3.6 | 17.8 | 4 | 395.38 | 0.3536 |

In addition, it can improve the efficiency of experimental design. Based on the screening results, 77 RSM test spaces are established as shown in Table 3.

After the experimental design space is established using RSM [12, 13]. It can also efficiently build polynomial regression models to fit the relationship among thrust force, thrust fluctuation, and parameters, which can be expressed as follows:

$$Y(X) = f(x_1, x_2, \ldots, x_k) \tag{7}$$

$Y(X)$ is a continuously differentiable objective function, which is simulated using a second-order polynomial model based on the relationship between the significant parameters of the motor and the performance to be optimized in this paper, expressed as:

$$y = \beta_0 + \sum_{i=1}^{n} \beta_i x_i + \sum_{i=1}^{n} \sum_{j=1}^{n} \beta_{ij} x_i x_j + \varepsilon \tag{8}$$

After organizing the above equation,

$$Y = X\beta + \varepsilon \tag{9}$$

where $Y$ is the matrix of the objective function consisting of thrust force and thrust fluctuation; $X$ is the significant parameter variable; $\beta$ is the coefficient of each item and satisfies $\beta = (X^T X)^{-1} X^T Y$.

In this paper, a second-order model is used to fit the relationship between six significant parameters and thrust force and thrust fluctuations. The RSM polynomial regression model for thrust force and thrust fluctuation was developed with the experimental data in Table 3 as:

$$
\begin{aligned}
y_1 = {} & -585.7 + 102.3x_1 + 26.6x_2 + 6.18x_3 + 30.73x_4 \\
& + 172.6x_5 + 19.36x_6 - 17.86x_1^2 + 1.05x_2^2 - 0.353x_3^2
\end{aligned}
$$

$$
\begin{aligned}
& -1.302x_4^2 - 17.87x_5^2 - 0.2159x_6^2 + 0.849x_1x_2 \\
& + 0.178x_1x_3 + 0.340x_1x_4 + 0.44x_1x_5 - 0.060x_1x_6 \\
& - 0.412x_2x_3 - 0.787x_2x_4 - 5.24x_2x_5 - 0.536x_2x_6 \\
& - 0.2633x_3x_4 - 0.382x_3x_5 + 0.0134x_3x_6 + 2.313x_4x_5 \\
& + 0.2420x_4x_6 - 3.014x_5x_6 \tag{10}
\end{aligned}
$$

$$
\begin{aligned}
y_2 = {} & 3.064 + 0.034x_1 - 0.141x_2 - 0.0038x_3 - 0.1923x_4 \\
& - 0.348x_5 - 0.0483x_6 - 0.0072x_1^2 + 0.0099x_2^2 \\
& - 0.00022x_3^2 + 0.00559x_4^2 + 0.0247x_5^2 + 0.000500x_6^2 \\
& - 0.00379x_1x_2 - 0.00067x_1x_3 + 0.00043x_1x_4 \\
& - 0.00071x_1x_5 + 0.000104x_1x_6 + 0.00098x_2x_3 \\
& + 0.00176x_2x_4 + 0.00513x_2x_5 + 0.001536x_2x_6 \\
& + 0.000746x_3x_4 - 0.00219x_3x_5 - 0.000043x_3x_6 \\
& + 0.00256x_4x_5 - 0.000092x_4x_6 + 0.005900x_5x_6 \tag{11}
\end{aligned}
$$

The degree of model strength must be assessed once a regression model has been developed. The coefficient of determination $R^2$ is an indicator to evaluate the fitting degree of the model, with values closer to 1, indicating a more effective model. The Root Mean Square Error (RMSE) is an indicator for evaluating the accuracy of the model's prediction, which reflects the difference between the predicted and the real values, and the expressions of the following expressions for both are as follows:

$$RMSE = \sqrt{\frac{1}{n} \sum_{i=1}^{n} (y_i - \hat{y}_i)^2} \tag{12}$$

$$R^2 = 1 - \frac{\sum (y_i - \hat{y}_i)^2}{\sum (y_i - \bar{y})^2} \tag{13}$$

**TABLE 3**. Taguchi method experimental space.

| Tests | $h_1$ | $h_2$ | $h_4$ | $h_5$ | $h_{pm}$ | $w_{pm}$ | $F_e$ | $F_{rip}$ |
|-------|-------|-------|-------|-------|----------|----------|-------|-----------|
| 1 | 3.6 | 3.6 | 9.7 | 18 | 2 | 40 | 343.43 | 0.1636 |
| 2 | 2.4 | 3.6 | 5.6 | 13.5 | 3 | 30 | 350.12 | 0.1788 |
| 3 | 1.2 | 3.6 | 1.5 | 9 | 4 | 20 | 249.36 | 0.4549 |
| ... | ... | ... | ... | ... | ... | ... | ... | ... |
| 76 | 3.6 | 2.4 | 5.6 | 13.5 | 3 | 30 | 388.25 | 0.1849 |
| 77 | 2.4 | 2.4 | 5.6 | 18 | 3 | 30 | 392.30 | 0.1785 |

**TABLE 4**. Evaluation of regression models.

| Evaluation metrics | $R^2$ | $RMSE$ |
|--------------------|-------|--------|
| Thrust force $F_e$ | 0.98375 | 8.077 |
| Thrust fluctuation $F_{rip}$ | 0.90059 | 0.048 |

**TABLE 5**. Optimal size of significant structural parameters.

| Parameters | $h_1$ | $h_2$ | $h_4$ | $h_5$ | $h_{pm}$ | $w_{pm}$ |
|------------|-------|-------|-------|-------|----------|----------|
| Size (mm) | 1.95 | 1.50 | 16.45 | 3.236 | 31.31 | 2.72 |



**FIGURE 8**. MOGOA flow chart.

where $y_i$ is the actual value; $\hat{y}_i$ is the model predicted value; $\bar{y}$ is the mean value; and $n$ is the number of tests.

After the establishment of the regression model, the model is evaluated simultaneously using both $R^2$ and $RMSE$. As seen in Table 4, the established regression model can meet the requirements of accuracy together with the subsequent parameter optimization search.

# 5. CO-OPTIMIZATION MODEL AND PERFORMANCE COMPARISON

## 5.1. Optimization Model

Based on the establishment of the polynomial regression model of RSM, multi-objective grasshopper optimization algorithm (MOGOA) is introduced to carry out iterative optimization of the model to achieve the co-optimization of thrust force and thrust fluctuation. MOGOA is a biomimetic optimization algorithm proposed in 2017, which performs the global search and iterative optimization by mimicking different behavioral performances of grasshoppers in different growth cycles [14, 15].

In a multi-objective optimization problem, each grasshopper individual searches near an optimal solution, continuously updating the optimal solution through search behavior until the stopping condition is met. Through continuous iteration, non-dominated solutions can be obtained, which are not dominated by other solutions and correspond to different solutions. The basic flow of MOGOA is shown in Fig. 8, depicting the process of obtaining non-dominated solutions through the iterative search and update of the optimal solution.

Equations (10) and (11) are iteratively optimized as the objective functions of MOGOA, and the obtained iteration results are shown in Fig. 9. As can be seen in Fig. 9, the thrust fluctuation increases gradually as the average thrust force of the motor increases.
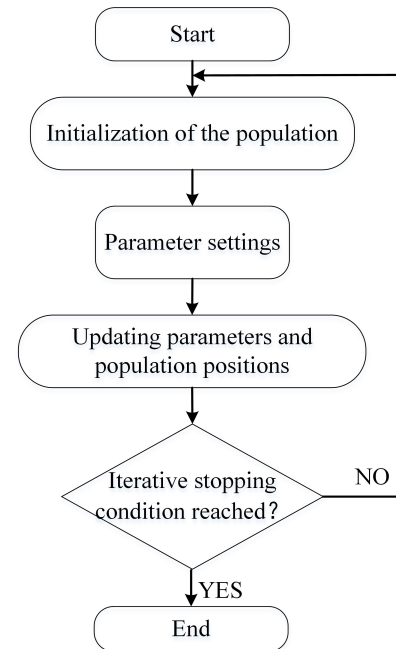
In the resulting Pareto frontiers, the two properties of thrust force and thrust fluctuation are considered, and a suitable one is selected as the optimal solution, corresponding to the dimensions of the six significant structural parameters as shown in Table 5.

## 5.2. Performance Comparison

Simulation and experiments are carried out to verify the derived parameter sizes for comparison using FEA, while ensuring that other parameters remain unchanged. Fig. 10 shows the comparison of the no-load induced voltage. The three-phase induced voltage amplitudes of A, B, and C are 29.68 V, 30.54 V, and 29.31 V, with an increase of 11.57 V, 12.29 V, and 11.08 V. The increase in no-load induced voltages improves the energy conversion efficiency of the motor. Fig. 11 shows the harmonic analysis of phase A. The harmonic distortion rate is reduced from 6.27 to 3.91%. The decreased harmonic distortion rate improves stability and reliability of motor operation.

Figure 12 shows the comparison of thrust force and detent force before and after optimization of LSDLFSPM motor structural parameters. The thrust force increased from 261.33 N to 415.92 N, resulting in an improvement of 154.59 N. Additionally, the detent force decreased from 41.0034 N to 25.80 N, reducing by 15.2034 N. Furthermore, the thrust fluctuation reduced from 36.19% to 15.91%, showing a reduction of 20.28%. The FEA results indicate that the performance of the LSDLFSPM motor is enhanced through the optimization of its structural parameters, as discussed in this paper.

Figure 13 illustrates the comparison of the air gap magnetic density, which is optimized to increase from 1.1 T to 1.65 T. It is also illustrated that after performing the parameter optimization, the motor has higher magnetic field strength and output performance.
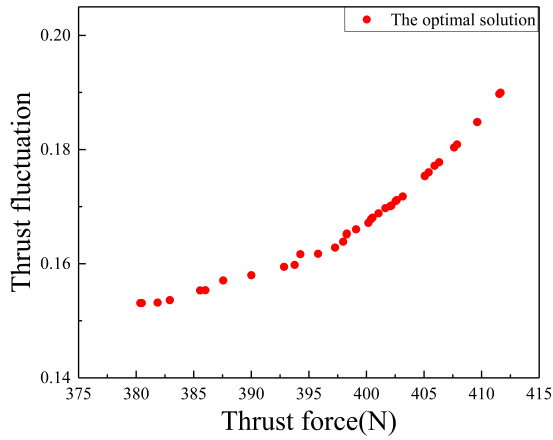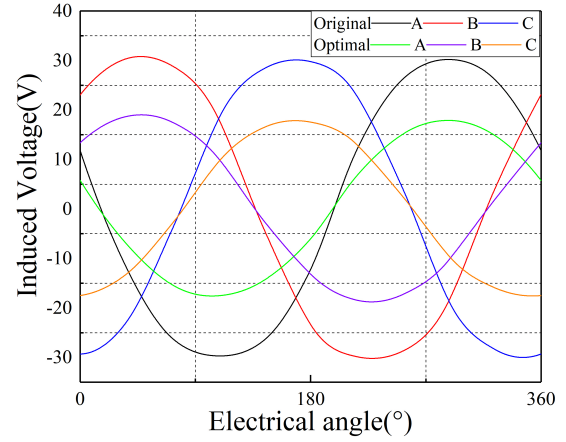
**FIGURE 9**. Results of MOGOA iteration.
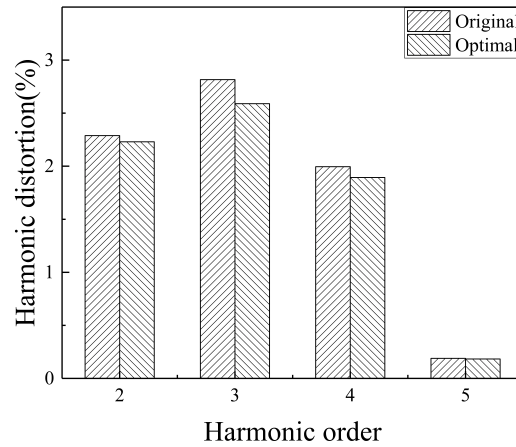


**FIGURE 10**. Induced voltage comparison.



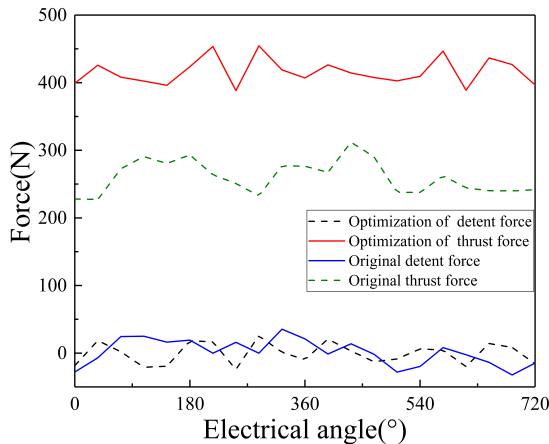**FIGURE 11**. Comparison of harmonic analysis.



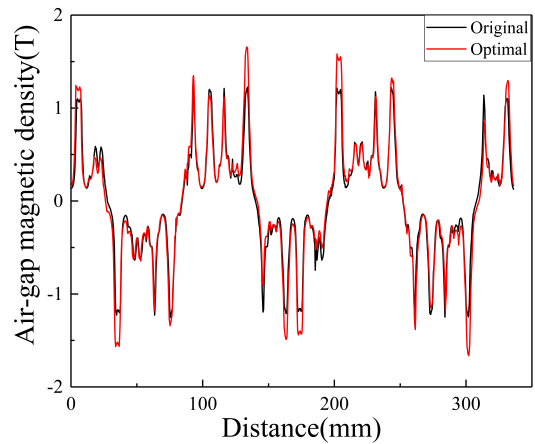**FIGURE 12**. Comparison of thrust and detent force.



**FIGURE 13**. Air gap magnetic density comparison.

## 6. CONCLUSION

In this paper, based on prior research on LSDLFSPM, a comprehensive optimization method is proposed utilizing sensitivity analysis via Taguchi method, RSM for experimental space and regression model construction, combined with MOGOA optimization, and verified by FEA experiments. This method aims to enhance the no-load induced voltages, minimize A-phase harmonic distortion rate, boost output average thrust force, reduce thrust fluctuation, lower detent force, and optimize permanent magnet usage of the LSDLFSPM. The results demonstrate a 154.59 N increase in output average thrust force, a 20.28% reduction in thrust fluctuation, a 15.2034 N decrease in detent force, and 29.03% reduction in permanent magnet usage. This method achieves synergistic optimization of thrust force and thrust fluctuation, enhancing operational stability and output performance of the motor.

## REFERENCES

[1] Zhou, H., X. Wang, Z. Zhang, and J.-A. Duan, "A novel thrust force test method for a class of precision noncontact linear motion actuators," *IEEE Transactions on Industrial Electronics*, Vol. 66, No. 7, 5383–5391, Jul. 2019.

[2] Hu, C., H. Cui, X. Li, X. Liu, and S. Huang, "Thrust characteristic improvement of permanent magnet linear synchronous motor based on multiobjective optimization," in *2021 13th International Symposium on Linear Drives for Industry Applications (LDIA)*, 1–5, Wuhan, China, 2021.

[3] Zhao, W., A. Ma, J. Ji, X. Chen, and T. Yao, "Multiobjective optimization of a double-side linear Vernier PM motor using response surface method and differential evolution," *IEEE Transactions on Industrial Electronics*, Vol. 67, No. 1, 80–90, Jan. 2020.

[4] Wang, Q., K. Wang, Y. Hu, D. Zeng, and J. Wang, "Global optimization of a complementary and modular linear flux-switching permanent magnet motor applied for urban rail transit to reduce normal force," in *2023 14th International Symposium on Linear Drives for Industry Applications (LDIA)*, 1–4, Hannover, Germany, 2023.

[5] Zhong, Z., QinghaoXiao, X. Wang, M. Yang, and Y. Wang, "Optimal design of doubly-fed linear motor for high speed maglev train based on improved genetic algorithm," in *2023 IEEE International Conference on Mechatronics and Automation (ICMA)*, 2089–2094, Harbin, Heilongjiang, China, 2023.

[6] Wang, K., Y. Hu, Q. Wang, and Q. Ge, "Optimization of secondary iron of homopolar linear synchronous motor for traction application based on finite element method and regression model," in *2023 5th Asia Energy and Electrical Engineering Symposium (AEEES)*, 453–459, Chengdu, China, 2023.

[7] Shiri, A. and A. Tessarolo, "Normal force elimination in single-sided linear induction motor using design parameters," *IEEE Transactions on Transportation Electrification*, Vol. 9, No. 1, 394–403, Mar. 2023.

[8] Wen, C., Q. Zhao, M. Li, J. Liu, M. Li, and X. Zhao, "Multiobjective optimization based on hyperparameter random forest regression for linear motor design," *International Journal of Machine Learning and Cybernetics*, Vol. 13, No. 10, 2929–2942, 2022.

[9] Cheng, M., P. Han, and W. Hua, "General airgap field modulation theory for electrical machines," *IEEE Transactions on Industrial Electronics*, Vol. 64, No. 8, 6063–6074, Aug. 2017.

[10] Liu, Q., H. Yu, M. Hu, C. Liu, J. Zhang, L. Huang, and S. Zhou, "Cogging force reduction of double-sided linear flux-switching permanent magnet machine for direct drives," *IEEE Transactions on Magnetics*, Vol. 49, No. 5, 2275–2278, May 2013.

[11] Wang, Y., J. Du, and Z. Hou, "Optimization and performance investigation of high precision permanent magnet linear motor," in *2022 25th International Conference on Electrical Machines and Systems (ICEMS)*, 1–6, Chiang Mai, Thailand, 2022.

[12] Chen, Q., Y. Fan, Y. Lei, and X. Wang, "Multi objective optimization design of unequal halbach array permanent magnet vernier motor based on optimization algorithm," in *2021 IEEE Energy Conversion Congress and Exposition (ECCE)*, 4220–4225, Vancouver, BC, Canada, 2021.

[13] Kim, W.-H., C.-W. Kim, H.-S. Shin, S.-S. Jeong, and J.-Y. Choi, "Optimal design of short-stroke linear oscillating actuator for minimization of side force using response surface methodology," *IEEE Transactions on Magnetics*, Vol. 58, No. 2, 8201905, Feb. 2022.

[14] Saremi, S., S. Mirjalili, and A. Lewis, "Grasshopper optimisation algorithm: Theory and application," *Advances in Engineering Software*, Vol. 105, 30–47, Mar. 2017.

[15] Mirjalili, S. Z., S. Mirjalili, S. Saremi, H. Faris, and I. Aljarah, "Grasshopper optimization algorithm for multi-objective optimization problems," *Applied Intelligence*, Vol. 48, 805–820, 2018.